# Bicircular High-Harmonic Spectroscopy Reveals Dynamical Symmetries of Atoms and Molecules



**Author(s):**
Baykusheva, Denitsa; Ahsan, Md Sabbir; Lin, Nan; Wörner, Hans Jakob

**Publication date:**
2016

**Permanent link:**
https://doi.org/10.3929/ethz-a-010625328



**Originally published in:**
Physical Review Letters 116(12), https://doi.org/10.1103/PhysRevLett.116.123001

# Bicircular High-Harmonic Spectroscopy Reveals Dynamical Symmetries of Atoms and Molecules

Denitsa Baykusheva, Md Sabbir Ahsan, Nan Lin, and Hans Jakob Wörner*
*Laboratorium für Physikalische Chemie, ETH Zürich, Vladimir-Prelog-Weg 2, 8093 Zürich, Switzerland*
(Received 6 January 2016; published 24 March 2016)

We introduce bicircular high-harmonic spectroscopy as a new method to probe dynamical symmetries of atoms and molecules and their evolution in time. Our approach is based on combining a circularly polarized femtosecond fundamental field of frequency $\omega$ with its counterrotating second harmonic $2\omega$. We demonstrate the ability of bicircular high-harmonic spectroscopy to characterize the orbital angular momentum symmetry of atomic orbitals. We further show that breaking the threefold rotational symmetry of the generating medium—at the level of either the ensemble or that of a single molecule—results in the emission of the otherwise parity-forbidden frequencies $3q\omega$ ($q \in \mathbb{N}$), which provide a background-free probe of dynamical molecular symmetries.

DOI: 10.1103/PhysRevLett.116.123001

Symmetry is a fundamental concept in science and plays a central role in our understanding of matter. Its close connection to conservation laws has been established in Noether's theorem [1]. Symmetry is also at the origin of selection rules that govern spectroscopy. These rules have been essential in determining molecular structures [2,3]. Access to symmetry on subfemtosecond time scales would open new avenues in time-resolved spectroscopy. Symmetry breaking is the source of a myriad of important physical effects. Famous examples include parity violation through the weak nuclear force, which results in energy differences between enantiomers of a chiral molecule [4], and the Jahn-Teller effect, which is the key to understanding the structure and dynamics of many molecules, transition-metal complexes, and solids [5,6].

Whereas the potential of high-harmonic spectroscopy (HHS) to probe the structure and dynamics of matter on the subfemtosecond and subangstrom scales has been well established [7–14], its ability to probe the symmetry of the medium on these time and length scales has not been addressed. High-harmonic generation from a linearly polarized driver is sensitive to inversion symmetry, the breaking of which leads to emission of even harmonics [15,16] that characterize the time-dependent electronic asymmetry of the studied sample [14,17]. In this Letter, we generalize the sensitivity of HHS to rotational symmetries of atoms and molecules and their time-dependent breaking by introducing bicircular HHS (BHHS), driven by a circularly polarized fundamental field of frequency $\omega$ and its counterrotating second harmonic $2\omega$. This scheme, which was theoretically proposed [18–21] and experimentally demonstrated [22] nearly two decades ago, has only recently been fully characterized and exploited as a light source [23,24]. Here, we establish the principles of self-probing spectroscopy based on this scheme and introduce the theoretical foundations for its interpretation. The time-dependent electric field driving high-harmonic emission describes a Lissajous figure with a threefold spatiotemporal symmetry, resembling a clover leaf [see Fig. 1(a)]. This field causes ionization, electron acceleration, and

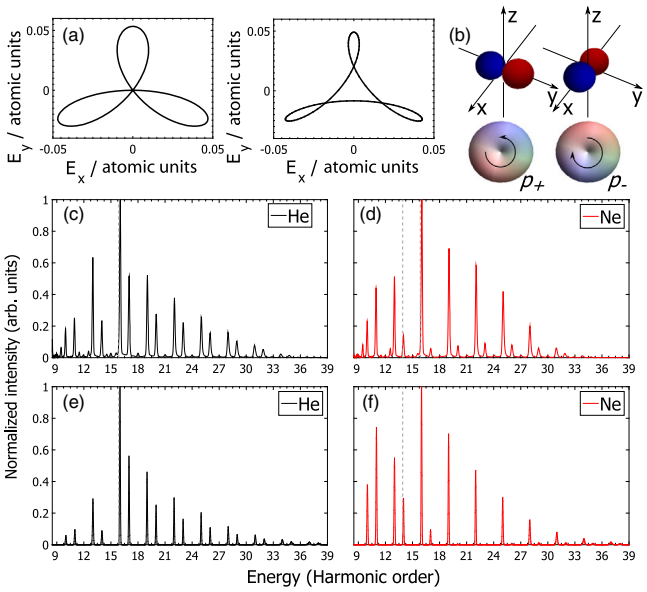


FIG. 1. Sensitivity of BHHS to electronic symmetry. (a) Lissajous curves of the electric field amplitude for one optical cycle of the fundamental field. The field amplitude ratio of the two drivers (800 nm/400 nm) is 1:1 in the left and 4:3 in the right-hand panel. (b) Illustration of the $p$ orbitals of neon in the Cartesian ($p_x$, $p_y$) and the spherical ($p_+$, $p_-$) basis. (c),(d) Experimental high-harmonic spectra generated in helium (c) and neon (d) under identical conditions. (e),(f) Results of 3D TDSE calculations for helium and neon. The dashed lines indicate the position of the first ionization threshold. The TDSE calculation employs a RCP field (800 nm) and a LCP 400 nm field with intensities of $3.0 \times 10^{14}$ and $1.8 \times 10^{14}$ W/cm$^2$, respectively. The pulse is modeled as a 15-cycle cos$^2$ pulse.

 

recombination three times per optical cycle of the fundamental field. When acting on an isotropic medium, the dynamical symmetry of the electric field translates into the emission of a comb of harmonics from which every third one, with frequency $3q\omega$, is missing. The explanation of these selection rules has recently attracted considerable interest [23,25–27].

We demonstrate that this property induces sensitivity to symmetry at two levels—the single-particle and the ensemble level. We show that the symmetry of atomic orbitals translates into pronounced variations of the relative intensities of allowed neighboring harmonics $3q+1$ and $3q+2$. Further, starting from isotropic gas-phase samples and imposing macroscopic order that violates the threefold symmetry of the driving field leads to the generation of forbidden $3q$ harmonic orders, which provide a background-free probe of the dynamic system under study. In addition, BHHS is shown to be sensitive to the instantaneous symmetry of molecules, which is used to probe internal dynamics occurring at the single-molecule level.

The experimental setup consists of a chirped-pulse amplified Ti:sapphire laser system and a vacuum chamber for the generation and characterization of high-harmonic radiation. The 1 kHz laser system delivers linearly polarized 25 fs pulses centered at 800 nm with a bandwidth of 50 nm. A portion of the beam serves as the pump arm for the pump-probe experiment, whereby a pair of thin-film-polarizer plates and wave plates is introduced for a fine adjustment of the intensity. The remaining part of the beam passes a 100-$\mu$m-thick $\beta$-BBO crystal for frequency doubling. The second harmonic is centered around 400 nm. The two frequencies are separated and temporally synchronized in a Mach-Zehnder-type interferometer. The polarization of each beam is set to nearly circular via a combination of achromatic zero-order half- and quarter-wave plates. After recombination, the two collinear beams are focused by a spherical Al mirror ($f/50$ or $f/40$) into the vacuum chamber, where they intersect a thin atomic or molecular beam generated by supersonic expansion in vacuum. This configuration minimizes the effects of phase mismatch and reabsorption, leading to the observation of a quasi-single-atom response. The distance of the focus and the orifice ($\oslash = 250$ $\mu$m) of the nozzle is kept at 0.1 cm or at 0.5–0.8 cm, depending on the requirements concerning the rotational temperature. Harmonic radiation is recorded using an extreme ultraviolet (XUV) grating, a microchannel plate detector, and a charge-coupled device camera.

Figures 1(c) and 1(d) display high-harmonic spectra generated in helium or neon under identical conditions ($I_\omega \approx 3.3\times10^{14}$ W/cm$^2$, $I_{2\omega} \approx 1.7\times10^{14}$ W/cm$^2$). In contrast to He, the spectra generated in Ne display a pronounced asymmetry in the intensity distribution of the $3q+1$ and $3q+2$ harmonic orders. As we show below, this observation results from the different symmetries of the highest-occupied orbitals ($s$ versus $p$). Our observations confirm the recent theoretical prediction made in Ref. [28]. Previous work has shown that careful manipulation of the phase-matching conditions can be used to modify the relative intensities of neighboring high harmonics [24]. However, the positioning of the focus well before the gas jet as well as the very thin atomic beam employed in our experiment provide a configuration deliberately aimed at excluding the influence of propagation effects. The detailed analysis of the phase-matching criteria presented in the Supplemental Material [Sec. I [29]] indicates that macroscopic effects can safely be neglected in our experiments.

In the following, we describe a simple model that quantitatively accounts for the experimental observations. For this, we resort to the spherical-basis representation of the three degenerate $p$ orbitals of Ne: $p_+ = -p_x/\sqrt{2} - ip_y/\sqrt{2}$, $p_- = p_x/\sqrt{2} - ip_y/\sqrt{2}$, $p_0 = p_z$ [Fig. 1(b)]. Since the $p_0$ orbital has a node in the polarization plane of the electric field, its contribution to the harmonic emission is negligible (see also Fig. S2 of Supplemental Material [29]). Here and in the remainder of this Letter, we assume without loss of generality, that the driving field consists of a right-circularly polarized (RCP) fundamental and a left-circularly polarized (LCP) second harmonic. In this configuration, an electron in a $p_+$ orbital ($m=+1$) circulates in the same sense as the fundamental field, while the $p_-$ orbital ($m=-1$) is counterrotating.

Following the reasoning behind the three-step model [48] and the factorization of the high-harmonic-generation (HHG) process [49–51], we treat the HHG process as a chronological sequence of ionization, propagation, and recombination steps. We first study the ionization yields from the three $p$ orbitals. The solution of the 3D time-dependent Schrödinger equation (TDSE) (Supplemental Material, Sec. II [29]) shows that, in contrast to the case of one-color circularly polarized fields [52–54], ionization from the corotating orbital $p_+$ is favored, but only by a very small amount [$\sim$1% under the conditions of Fig. 1(f)].

By invoking the principle of detailed balance [55], photorecombination (PR) can be treated as the time reverse of photoionization [10,51]. A symmetry analysis shows that harmonics $3q+1$ are RCP, whereas the $3q+2$ harmonics are LCP (or, in general, corotating and counterrotating with respect to the fundamental field, respectively) [20]. High-harmonic emission at these frequencies can therefore be described as the time-reversed single-photon ionization by correspondingly polarized radiation. We therefore represent the intensity of each harmonic as the coherent sum of two contributions arising from the $p_+$ and $p_-$ orbitals. Conservation of angular momentum implies that photorecombination to the orbital rotating in the direction opposite to the emitted field can occur from both $s$- and $d$-wave continua whereas the continuum symmetry is restricted to $d$ waves for the corotating orbital (Supplemental Material, Sec. III [29]). The coherent

addition of these terms can give rise to constructive or destructive interference, depending on the phase of the angular part of the matrix elements.

In contrast to HHG driven by linearly polarized fields, the angle between the direction of ionization and that of recollision can cover a large range (10°–130° in our experiments, Fig. S3(b) of Supplemental Material [29]). The angular part of the photorecombination matrix elements therefore plays a key role. Taking all of these aspects into account, our numerical calculations (Figs. S4 and S5 of Supplemental Material [29]) show that the $3q+2$ harmonic orders of Ne are suppressed in the spectral region of H16-H30 by a destructive interference between the contributions of the corotating and counterrotating orbitals, explaining both the experimental observations in Fig. 1(d) and the TDSE calculations in Fig. 1(f).

A further implication of our analysis is the fact that the orbital symmetry ($s$ versus $p$) is not the only determining factor for the observed intensity distribution. The experimentally obtained [Fig. S7(a) [29]] and calculated [Fig. S7(b) [29]] high-harmonic spectra of argon, another atom with a highest-occupied orbital of $p$ symmetry, display a very different intensity distribution compared to neon. We show (Supplemental Material, Sec. III [29]) that this behavior is the consequence of $\sim\pi$ rad phase difference between the radial matrix elements of the $s$ and $d$ continua of Ar below the Cooper minimum (53 eV).

These results can be summarized in the following picture. When orbitals of $s$ symmetry dominate HHG, only one partial wave of the continuum ($p$) contributes to the emission, there is no possibility for destructive interference, and, therefore, the intensities of neighboring harmonic orders are similar. When orbitals with $\ell \geq 1$ dominate HHG, two partial waves contribute to emission from the orbital rotating opposite to the driving electric field, which enables both constructive and destructive interferences. The location of these interferences depends on the relative phase of the radial matrix elements and the angle of recollision. Therefore, the intensity ratio of neighboring harmonics may substantially deviate from 1, as observed in Ne and predicted to occur at energies above the Cooper minimum in Ar (Supplemental Material, Sec. III, and Fig. S5 [29]).

We now outline how BHHS can be applied to study time-dependent molecular symmetries. The rationale behind our approach is to break the symmetry of the medium in a controlled way and to follow the intensity evolution of the symmetry-forbidden $3q$ harmonics, thus utilizing them as a background-free probe. We choose BHHS of aligned $N_2$ molecules to showcase the potential of this idea. A nonresonant linearly polarized laser pulse ($0.6 \pm 0.1 \times 10^{14}$ W/cm$^2$) is used to excite a rotational wave packet in gaseous $N_2$ molecules via impulsive stimulated Raman scattering. The rotational distribution is interrogated by the bicircular probe ($I_\omega \approx 2.7 \times 10^{14}$ W/cm$^2$, $I_{2\omega} \approx 1.5 \times 10^{14}$ W/cm$^2$) around a delay of 4 ps, which corresponds to the first rotational half-revival. The induced alignment is quantified in terms of the expectation value of $\cos^2(\theta)$ [Fig. 2(b), with $\theta$ being the angle between the laser polarization direction and the molecular axis], obtained by solving the rotational time-dependent Schrödinger equation using the experimental pulse parameters. Figure 2(c) provides a visual interpretation of the macroscopic symmetry-breaking concept. The transient alignment imposed upon the molecular ensemble is axially symmetric with respect to the polarization vector of the pump [taken along the $X$ axis in Fig. 2(c)] and the spatial symmetry of the ensemble around the revival maximum (minimum) [4.0 ps (4.3 ps)] can be classified as $D_{\infty h}$. At pump-probe delays outside of the fractional revivals, the distribution is close to spherically symmetric ($K$). However, in the presence of the bicircular probe field, the overall sample plus field symmetry is reduced to $C_3$ (isotropic sample) or $C_1$ (aligned sample). The deviation of threefold symmetry in the aligned case lifts the selection rules and allows for the emission of harmonics at all integer multiples of $\omega$ [27]. This effect is clearly visible in Fig. 2(a). At the alignment maximum ($C_1$ symmetry) the harmonic orders $3q$ have intensities comparable to those of the neighboring harmonics, whereas a nearly isotropic distribution ($C_3$ symmetry) leads to the expected near-complete suppression of the $3q$ orders.

The variation of the intensity with the pump-probe delay for a selected set of harmonic orders is presented in Fig. 2(d), with the harmonics $3q$ shown in the leftmost column and several $(3q \pm 1)$ orders displayed in the third column. The harmonics $3q$ display a very pronounced modulation with a contrast $> 10$, whereas the remaining

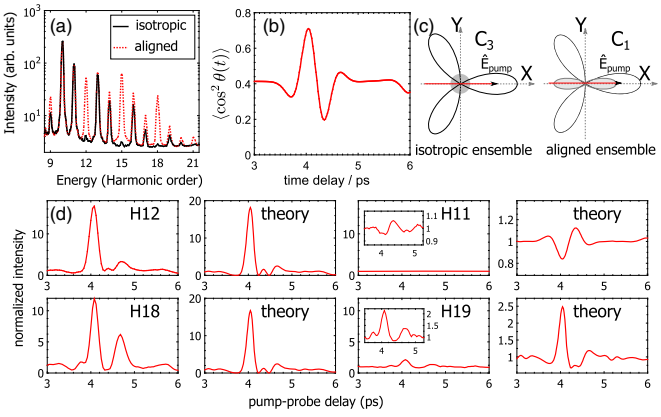


FIG. 2. Probing the ensemble symmetry of a rotational wave packet. (a) Harmonic spectra of aligned (4.0 ps) and quasi-isotropic (6.0 ps) $N_2$. (b) Plot of the calculated time evolution of the $\cos^2(\theta)$ expectation value. (c) Sketch of the dynamical symmetry (system plus electric field) for an isotropic ensemble ($C_3$ symmetry) and an aligned sample ($C_1$ symmetry). (d) Measured and calculated intensities of a selected range of harmonic orders in aligned $N_2$ as a function of the pump-probe delay.

harmonics display a weak modulation that inverts as a function of the harmonic order. We analyze these results by extending the approach introduced in the preceding section in the context of atoms to the molecular case. To account for the dependence of the PR-matrix elements [Fig. S7(b) [29]] on the molecular orientation, the BHHS process is treated on a subcycle time scale. Within one full cycle of the fundamental field, the sequence of ionization, propagation, and recombination is repeated three times, resulting in the emission of three temporally shifted attosecond bursts. In the case of an anisotropic molecular-axis distribution, the three bursts differ in amplitude and in phase. We therefore obtain the harmonic emission over one full cycle by first averaging the emission amplitude for one subcycle event over the calculated alignment distribution and subsequently adding the three contributions coherently. In the case of an isotropic axis distribution, this procedure leads to an exact cancellation of the harmonic orders $3q$. In the case of an aligned ensemble, recollision under different angles in the molecular frame removes the destructive interference of the $3q\omega$ frequency components, resulting in strong emission at these frequencies. We note that our model predicts a dependence of the harmonic intensities on the phase delay between the $\omega$ and $2\omega$ fields in the case of partially aligned samples. However, this effect could not be identified experimentally, most likely because of insufficient interferometric stability.

The results of our calculations are presented in the second ($3q$) and the last ($3q \pm 1$) columns of Fig. 2(d). The revival pattern of the $3q$ orders, consisting of a global maximum at 4.0 ps followed by two local maxima at 4.35 and 4.75 ps, is well reproduced by the model. Maxima in the high-harmonic emission reflect maximal deviations of the axis distribution from the threefold symmetry of the driving field [Fig. S7(d) [29]]. The global maximum at 4.00 ps corresponds to the sharp localization of the wave packet in the equatorial plane (defined with respect to the $\vec{k}$ vector of the bicircular field), while the two smaller maxima correspond to the symmetric splitting of the wave packet between the two poles at ≈4.3 ps and the subsequent relocalization in the polarization plane after 4.75 ps.

The set of $3q \pm 1$ harmonics presented in Fig. 2(d) display a progression from a minimum at 4.0 ps, followed by a maximum at 4.3 ps, to an inverted pattern. This results from an interplay between the orientational dependence of the photorecombination amplitudes and the alignment distribution. At energies below ≈27 eV (H17), photorecombination favors molecules aligned parallel to the probe $\vec{k}$ vector. The probability for a molecule to be found in such an orientation maximizes at 4.3 ps, which is consistent with the experimentally observed signal of H11. In the region between 26 and 37 eV (H17–H23), the PR cross sections exhibit a local maximum at 90° and the modulation pattern inverts. We show in the Supplemental Material [29] that this behavior is a consequence of the $2\sigma_g \rightarrow k\sigma_u$ photoelectron continuum shape resonance of $N_2$.

Finally, we show that BHHS can be applied to probe dynamical symmetry breaking induced by intramolecular dynamics. The $SF_6$ molecule possesses Raman-active vibrational modes of $A_{1g}$ (≈775 $cm^{-1}$), $E_g$ (≈643 $cm^{-1}$), and $T_{2g}$ (≈525 $cm^{-1}$) symmetries [Fig. 3(a)]. We use a strong linearly polarized 28 fs pulse ($6.5 \pm 0.4 \times 10^{13}$ W/$cm^2$) preceding the bichromatic probe ($I_\omega \approx 2.2 \times 10^{14}$ W/$cm^2$, $I_{2\omega} \approx 1.3 \times 10^{14}$ W/$cm^2$) to impulsively excite these vibrational modes [56]. The $E_g$ mode is only weakly Raman active and does not appear in the current

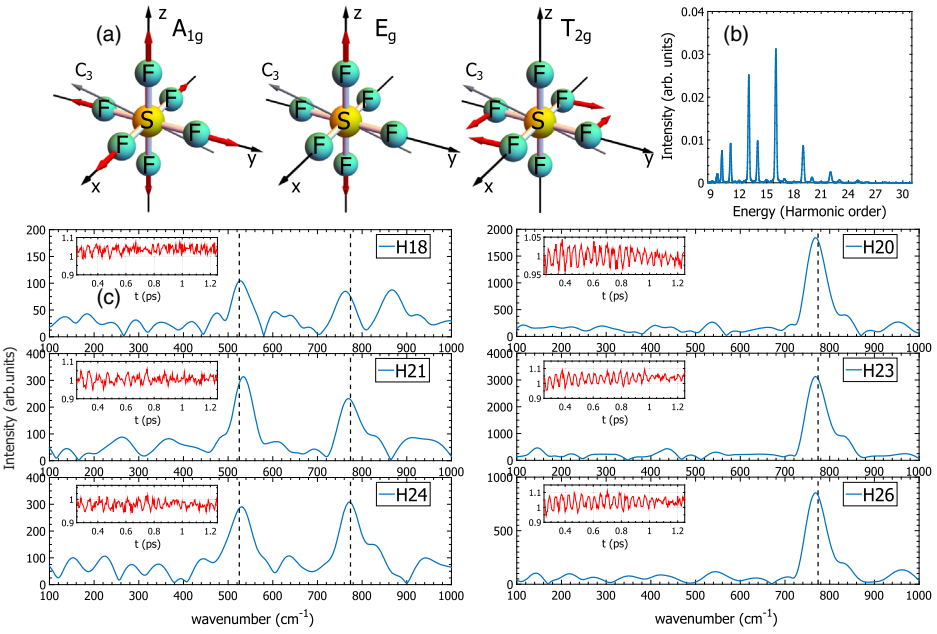


FIG. 3. Distinction of symmetry-breaking and symmetry-preserving molecular vibrations. (a) Sketch of the structure of the $SF_6$ molecule. The blue arrows indicate the nuclear distortions along the three Raman-active modes. (b) HHG spectrum of $SF_6$ in the absence of the pump pulse. (c) Fourier spectra of the harmonic signals obtained after excitation by a linearly polarized excitation pulse. The spectra in the left column pertain to the parity-forbidden $3q$ harmonics. The insets contain the corresponding temporal profiles.

experiment, as evident from Fig. 3(c). Vibrations along the totally symmetric $A_{1g}$ mode preserve the $O_h$ symmetry of the molecule and, therefore, also its $C_3$ axial symmetry. In contrast, the $T_{2g}$ vibrations break this symmetry, as illustrated in Fig. 3(c). Experimentally, we find that the intensities of the allowed harmonics $3q+1$ and $3q+2$ are only modulated at the frequency of the $A_{1g}$ symmetry-preserving mode. Interestingly, this observation differs from previous HHS experiments using linear drivers [56–58]. In all of those experiments, the $A_{1g}$ and $T_{2g}$ modes were observed with comparable contrasts, the $T_{2g}$ mode even dominating in some harmonic orders. This comparison shows that the self-probing properties of BHHS differ from those of traditional HHS. Most importantly, however, BHHS systematically discriminates between symmetry-breaking and symmetry-preserving vibrations. This is very clearly demonstrated through the fact that the intensities of the forbidden harmonics $3q$ are additionally modulated at the frequency of the symmetry-breaking $T_{2g}$ modes.

Bicircular HHS as introduced in this Letter has a broad range of innovative applications. The sensitivity of the polarization of the emitted harmonic radiation to the angular momentum of the highest-occupied orbital of the generating medium provides a convenient pathway for isolating XUV radiation with a specific helicity. Potential applications of this aspect include the generation of isolated elliptically polarized attosecond pulses [28,59]. Extending BHHS to molecules, we demonstrated its extreme sensitivity to both electronic structure (shape resonance in $N_2$) and symmetry breaking at the ensemble level. Working with vibrationally excited molecules, we showed that BHHS discriminates between symmetry-breaking and symmetry-preserving modes. These principles can be applied as a background-free probe of symmetry-breaking process, such as the Jahn-Teller effect. The two-dimensional nature of the electron trajectories and the wider range of recollision angles spanned by the returning electron provide new pathways for developing the self-imaging aspect of HHS, which will give access to attosecond time scales. These properties are expected to extend to BHHS of solids [60,61], where it will open up promising directions, such as the time-resolved study of symmetry and symmetry breaking in crystals.

We gratefully acknowledge funding from an ERC Starting Grant (Project No. 307270-ATTOSCOPE) and the Swiss National Science Foundation via the National Centre of Competence in Research Molecular Ultrafast Science and Technology.

*hwoerner@ethz.ch; www.atto.ethz.ch

[1] E. Noether, Nachr. Ges. Wiss. Göttingen Math.-Phys. Kl. 235 (1918) [Transport Theory and Statistical Physics **1**, 186 (1971)].
[2] G. Herzberg, *Molecular Spectra and Molecular Structure, Vol. II. Infrared and Raman Spectra of Polyatomic Molecules* (Krieger Publishing Company, Malabar, FL, 1991).
[3] G. Herzberg, *Molecular Spectra and Molecular Structure, Vol. III. Electronic Spectra and Electronic Structure of Polyatomic Molecules*, 2nd ed. (Krieger Publishing Company, Malabar, FL, 1991).
[4] M. Quack, Angew. Chem., Int. Ed. Engl. **41**, 4618 (2002).
[5] I. B. Bersuker, *The Jahn-Teller Effect* (Cambridge University Press, Cambridge, England, 2006).
[6] H. J. Wörner and F. Merkt, Angew. Chem., Int. Ed. Engl. **48**, 6404 (2009).
[7] J. Itatani, J. Levesque, D. Zeidler, H. Niikura, H. Pépin, J. C. Kieffer, P. B. Corkum, and D. M. Villeneuve, Nature (London) **432**, 867 (2004).
[8] M. Lein, Phys. Rev. Lett. **94**, 053004 (2005).
[9] S. Baker *et al.*, Science **312**, 424 (2006).
[10] T. Morishita, A.-T. Le, Z. Chen, and C. D. Lin, Phys. Rev. Lett. **100**, 013903 (2008).
[11] M. V. Frolov, N. L. Manakov, T. S. Sarantseva, M. Y. Emelin, M. Y. Ryabikin, and A. F. Starace, Phys. Rev. Lett. **102**, 243901 (2009).
[12] O. Smirnova, Y. Mairesse, S. Patchkovskii, N. Dudovich, D. Villeneuve, P. Corkum, and M. Y. Ivanov, Nature (London) **460**, 972 (2009).
[13] H. J. Wörner, J. B. Bertrand, D. V. Kartashov, P. B. Corkum, and D. M. Villeneuve, Nature (London) **466**, 604 (2010).
[14] P. M. Kraus *et al.*, Science **350**, 790 (2015).
[15] E. Frumker, C. T. Hebeisen, N. Kajumba, J. B. Bertrand, H. J. Wörner, M. Spanner, D. M. Villeneuve, A. Naumov, and P. B. Corkum, Phys. Rev. Lett. **109**, 113901 (2012).
[16] P. M. Kraus, A. Rupenyan, and H. J. Wörner, Phys. Rev. Lett. **109**, 233903 (2012).
[17] P. M. Kraus, D. Baykusheva, and H. J. Wörner, Phys. Rev. Lett. **113**, 023001 (2014).
[18] S. Long, W. Becker, and J. K. McIver, Phys. Rev. A **52**, 2262 (1995).
[19] T. Zuo and A. D. Bandrauk, J. Nonlinear Opt. Phys. Mater. **04**, 533 (1995).
[20] W. Becker, B. N. Chichkov, and B. Wellegehausen, Phys. Rev. A **60**, 1721 (1999).
[21] D. B. Milošević, W. Becker, and R. Kopold, Phys. Rev. A **61**, 063403 (2000).
[22] H. Eichmann, A. Egbert, S. Nolte, C. Momma, B. Wellegehausen, W. Becker, S. Long, and J. K. McIver, Phys. Rev. A **51**, R3414 (1995).
[23] A. Fleischer, O. Kfir, T. Diskin, P. Sidorenko, and O. Cohen, Nat. Photonics **8**, 543 (2014).
[24] O. Kfir *et al.*, Nat. Photonics **9**, 99 (2015).
[25] E. Pisanty, S. Sukiasyan, and M. Ivanov, Phys. Rev. A **90**, 043829 (2014).
[26] D. B. Milošević, J. Phys. B **48**, 171001 (2015).
[27] F. Mauger, A. D. Bandrauk, and T. Uzer, arXiv:1501.02557.
[28] L. Medišauskas, J. Wragg, H. van der Hart, and M. Y. Ivanov, Phys. Rev. Lett. **115**, 153001 (2015).
[29] See Supplemental Material at http://link.aps.org/supplemental/10.1103/PhysRevLett.116.123001, which includes Refs. [30–47], for details about the phase-matching, TDSE and photorecombination calculations.

[30] M. D. Morse, *Experimental Methods in Physical Sciences*, Atomic, Molecular, and Optical Physics: Atoms and Molecules Part B, Vol. 29 (Elsevier Inc., New York, 1996), Chap. 2, pp. 21–47.
[31] A. Börzsönyi, Z. Heiner, M. P. Kalashnikov, A. P. Kovács, and K. Osvay, Appl. Opt. **47**, 4856 (2008).
[32] E. Constant, D. Garzella, P. Breger, E. Mével, Ch. Dorrer, C. Le Blanc, F. Salin, and P. Agostini, Phys. Rev. Lett. **82**, 1668 (1999).
[33] T. Popmintchev, M.-C. Chen, A. Bahabad, M. Gerrity, P. Sidorenko, O. Cohen, I. P. Christov, M. M. Murnane, and H. C. Kapteyn, Proc. Natl. Acad. Sci. U.S.A. **106**, 10516 (2009).
[34] T. Popmintchev *et al.*, Science **336**, 1287 (2012).
[35] J. Samson and W. Stolte, J. Electron Spectrosc. Relat. Phenom. **123**, 265 (2002).
[36] X.-M. Tong and S.-I. Chu, Chem. Phys. **217**, 119 (1997).
[37] M. Murakami, O. Korobkin, and M. Horbatsch, Phys. Rev. A **88**, 063419 (2013).
[38] X. M. Tong and C. D. Lin, J. Phys. B **38**, 2593 (2005).
[39] H. G. Muller and F. C. Kooiman, Phys. Rev. Lett. **81**, 1207 (1998).
[40] H. A. Bethe and E. E. Salpeter, *Quantum Mechanics of One- and Two-Electron Atoms*, (Springer, New York, 1977).
[41] U. Fano, Phys. Rev. A **32**, 617 (1985).
[42] J. Zakrzewski, D. Delande, J.-C. Gay, and K. Rzążewski, Phys. Rev. A **47**, R2468 (1993).
[43] K. Rzążewski and B. Piraux, Phys. Rev. A **47**, R1612 (1993).
[44] D. Farrelly and T. Uzer, Phys. Rev. Lett. **74**, 1720 (1995).
[45] F. A. Gianturco, R. R. Lucchese, and N. Sanna, J. Chem. Phys. **100**, 6464 (1994).
[46] A. P. P. Natalense and R. R. Lucchese, J. Chem. Phys. **111**, 5344 (1999).
[47] J. Ortigoso, M. Rodríguez, M. Gupta, and B. Friedrich, J. Chem. Phys. **110**, 3870 (1999).
[48] P. B. Corkum, Phys. Rev. Lett. **71**, 1994 (1993).
[49] A.-T. Le, R. R. Lucchese, S. Tonzani, T. Morishita, and C. D. Lin, Phys. Rev. A **80**, 013401 (2009).
[50] M. V. Frolov, N. L. Manakov, T. S. Sarantseva, and A. F. Starace, J. Phys. B **42**, 035601 (2009).
[51] H. J. Wörner, H. Niikura, J. B. Bertrand, P. B. Corkum, and D. M. Villeneuve, Phys. Rev. Lett. **102**, 103901 (2009).
[52] X. Xie, A. Scrinzi, M. Wickenhauser, A. Baltuška, I. Barth, and M. Kitzler, Phys. Rev. Lett. **101**, 033901 (2008).
[53] I. Barth and O. Smirnova, Phys. Rev. A **84**, 063415 (2011).
[54] T. Herath, L. Yan, S. K. Lee, and W. Li, Phys. Rev. Lett. **109**, 043004 (2012).
[55] L. D. Landau and E. M. Lifshitz, *A Course on Theoretical Physics: Quantum Mechanics*, Vol. 3 (Pergamon Press, New York, 1965).
[56] N. L. Wagner, A. Wuest, I. P. Christov, T. Popmintchev, X. Zhou, M. M. Murnane, and H. C. Kapteyn, Proc. Natl. Acad. Sci. U.S.A. **103**, 13279 (2006).
[57] A. Ferré, D. Staedter, F. Burgy, M. Dagan, D. Descamps, N. Dudovich, S. Petit, H. Soifer, V. Blanchet, and Y. Mairesse, J. Phys. B **47**, 124023 (2014).
[58] A. Ferré *et al.*, Nat. Commun. **6**, 5952 (2015).
[59] F. Mauger, A. D. Bandrauk, A. Kamor, T. Uzer, and C. Chandre, J. Phys. B **47**, 041001 (2014).
[60] G. Vampa, T. J. Hammond, N. Thiré, B. E. Schmidt, F. Légaré, C. R. McDonald, T. Brabec, and P. B. Corkum, Nature (London) **522**, 462 (2015).
[61] T. T. Luu, M. Garg, S. Y. Kruchinin, A. Moulet, M. Th. Hassan, and E. Goulielmakis, Nature (London) **521**, 498 (2015).